

Research Note: A workaround for the corner problem in numerically exact non-reflecting boundary conditions

W.A. Mulder^{1,2*}

¹Shell Global Solutions International B.V., P.O. Box 38000, 1030 BN Amsterdam, The Netherlands, and ²Department of Geoscience & Engineering, Faculty of Civil Engineering and Geosciences, Delft University of Technology, P.O. Box 5048, 2600 GA Delft, The Netherlands

Received March 2020, revision accepted July 2020

ABSTRACT

Simulations of wave propagation in the Earth usually require truncation of a larger domain to the region of interest to keep computational cost acceptable. This introduces artificial boundaries that should not generate reflected waves. Most existing boundary conditions are not able to completely suppress all the reflected energy, but suffice in practice except when modelling subtle events such as interbed multiples. Exact boundary conditions promise better performance but are usually formulated in terms of the governing wave equation and, after discretization, still may produce unwanted artefacts. Numerically exact non-reflecting boundary conditions are instead formulated in terms of the discretized wave equation. They have the property that the numerical solution computed on a given domain is the same as one on a domain enlarged to the extent that waves reflected from the boundary do not have the time to reach the original truncated domain. With a second- or higher-order finite-difference scheme for the one-dimensional wave equation, these boundary conditions follow from a recurrence relation. In its generalization to two or three dimensions, a recurrence relation was only found for a single non-reflecting boundary on one side of the domain or two of them at opposing ends. The other boundaries should then be zero Dirichlet or Neumann. If two non-reflecting boundaries meet at a corner, translation invariance is lost and a simple recurrence relation could not be found.

Here, a workaround is presented that restores translation invariance by imposing classic, approximately non-reflecting boundary conditions on the other sides and numerically exact ones on the two opposing sides that otherwise would create the strongest reflected waves with the classic condition. The exact ones can also be applied independently. As a proof of principle, the method is applied to the two-dimensional acoustic wave equation, discretized on a rectangular domain with a second-order finite-difference scheme and first-order Enquist–Majda boundary conditions as approximate ones. The method is computationally costly but has the advantage that it can be reused on a sequence of problems as long as the time step and the sound speed values next to the boundary are kept fixed.

Key words: Acoustics, Computing aspects, Mathematical formulation, Seismics, Modelling.

INTRODUCTION

Modelling seismic wave propagation in a subset of the Earth requires truncation of the computational domain to the region

*Email: wim.mulder@shell.com

of interest. The resulting artificial boundaries should not generate reflected waves that were absent in the original problem. The large number of papers on the subject suggests that this cannot be considered a solved problem. Among the many reviews and comparison papers are those by Mitra *et al.* (1989), Tsynkov (1998), Tourrette and Halpern (2001), Givoli (2004), Hagstrom and Lau (2007), Bérenger (2015), Antoine *et al.* (2017) and Gao *et al.* (2017). Most existing boundary conditions are not able to completely suppress reflected energy, but may still suffice in practice. In some cases, for instance, when modelling interbed multiples, the reflected events may be too strong and a better method is required.

A subset of these boundary conditions is exact. Some involve an analytical solution in the region between the truncated domain and infinity, which is feasible if the problem is homogeneous or special enough that such a solution exists (Keller and Givoli, 1989; Deakin and Dryden, 1995; Givoli *et al.*, 1998). Others are based on Green's second identity (Ting and Miksis, 1986; Deakin and Dryden, 1995; van Manen *et al.*, 2007). Givoli and Cohen (1995) showed that the method of Ting and Miksis (1986) suffers from a weak instability that can be suppressed by adding some dissipation. Teng (2003) proposed a formulation based on boundary integrals, which after discretization becomes the local condition of Engquist and Majda (1979).

Losing exactness after discretization can be avoided if the partial differential equation (PDE) is discretized first and then an exact boundary condition is formulated. The result can be called a numerically exact non-reflecting boundary condition, to distinguish it from the earlier analytical methods. Note that on a computer, the finite number of digits for the representation of floating point numbers will produce round-off errors and exactness does not exist. The term will nevertheless be used with the silent assumption that the round-off errors are orders of magnitude smaller than the discretization error of the PDE.

Numerically exact non-reflecting boundary conditions produce a solution that is the same as a subset of one obtained on an enlarged domain with boundaries moved so far away that their reflected waves do not have time to reach the original domain. They were proposed in a preceding paper (Mulder, 2020) for a rectangular domain. Earlier, Sofronov and Podgornova (2006) considered a similar method for circular domains with polar coordinates and Fourier modes in the direction parallel to the boundary. The non-reflecting conditions are based on the boundary Green functions computed for the discretized PDE, called elementary kernels by Sofronov and Podgornova (2006).

In the one-dimensional case with a finite-difference approximation of second or higher order, the boundary conditions obey a recurrence relation. This observation, made in the preceding paper, significantly reduces the cost of computing the elementary kernels or boundary Green functions. In the generalization to more than one space dimension and on a rectangular domain, however, the derivation of a recurrence relation seems only to be feasible for a single non-reflecting boundary, or for two of them at opposing ends of the rectangular domain. The other boundaries should then be zero Dirichlet or Neumann. The reason is the assumed translation invariance in the direction perpendicular to the boundary. This property is lost in the presence of a corner where two non-reflecting boundaries meet. Then, a simple recurrence relation no longer seems to exist.

The workaround proposed here combines the exact boundary condition in one coordinate direction with a classic, approximately non-reflecting boundary condition (Engquist and Majda, 1979; Higdon, 1986, a.o.) in the other coordinate direction(s). This restores translation invariance at the expense of numerical exactness. Still, the method can be useful if the approximately non-reflecting boundary conditions produce too strong unwanted reflection events in one coordinate direction. This can happen, for instance, when modelling interbed multiples in marine examples with a shallow sea or in land examples with strong surface waves.

The method is described for the simplest case of the two-dimensional acoustic wave equation discretized with the lowest-order finite-difference scheme, combined with the lowest-order Engquist–Majda boundary conditions. Numerical tests are included.

METHOD

Discretization

The acoustic wave equation in two dimensions is given by

$$\frac{1}{\rho c^2} \frac{\partial^2 u}{\partial t^2} = \frac{\partial}{\partial x} \left(\frac{1}{\rho} \frac{\partial u}{\partial x} \right) + \frac{\partial}{\partial z} \left(\frac{1}{\rho} \frac{\partial u}{\partial z} \right) + f, \quad (1)$$

with a solution $u(t, x, z)$ depending on time t and position (x, z) in a given model with sound speed $c(x, z)$ and density $\rho(x, z)$. The source term $f(t, x, z)$ is typically of the form $w(t)\delta(x - x_s)\delta(z - z_s)$ for a point source at (x_s, z_s) with wavelet $w(t)$. The rectangular computational domain is defined by $[x_{\min}, x_{\max}] \times [z_{\min}, z_{\max}]$ and discretized on a grid with $N_x \times N_z$ points: $x_i = x_{\min} + (i - \frac{1}{2})\Delta x$, $i = 1, \dots, N_x$, and $z_j = z_{\min} + (j - \frac{1}{2})\Delta z$, $j = 1, \dots, N_z$, with grid spacings $\Delta x = (x_{\max} - x_{\min})/N_x$ and $\Delta z = (z_{\max} - z_{\min})/N_z$,

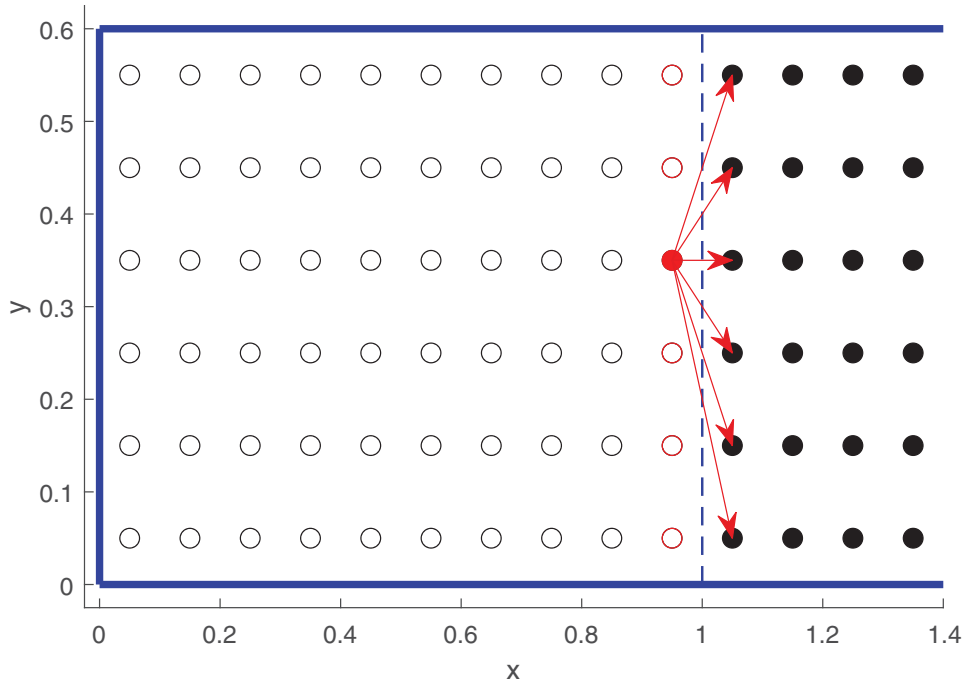


Figure 1 Enlarged domain with the grid points of the original domain drawn as open circles and those of the exterior as filled black circles. The boundaries on the left, top and bottom are, for instance, zero Dirichlet, and are drawn in blue. The discrete boundary Green function is the response in the exterior of a unit spike at time zero for a given grid point, marked as a filled red circle, on the non-reflecting boundary of the interior, otherwise indicated by red open circles. For a second-order scheme, only the values at exterior grid points next to the boundary are needed, as indicated by the arrows. With constant extrapolation of the material properties in the direction perpendicular to the boundary, the boundary Green functions are translation-invariant when stepping towards the right.

respectively. The standard second-order finite-difference scheme in space and time is

$$\begin{aligned} & \frac{1}{\rho_{i,j} c_{i,j}^2 \Delta t^2} \left(u_{i,j}^{n+1} - 2u_{i,j}^n + u_{i,j}^{n-1} \right) \\ &= \frac{1}{\Delta x^2} \left[(\rho_{i+1/2,j}^{-1} (u_{i+1,j}^n - u_{i,j}^n) - \rho_{i-1/2,j}^{-1} (u_{i,j}^n - u_{i-1,j}^n)) \right] \\ &+ \frac{1}{\Delta z^2} \left[\rho_{i,j+1/2}^{-1} (u_{i,j+1}^n - u_{i,j}^n) - \rho_{i,j-1/2}^{-1} (u_{i,j}^n - u_{i,j-1}^n) \right] + f_{i,j}^n. \end{aligned} \quad (2)$$

The average specific volumes are $\rho_{i+1/2,j}^{-1} = 2/(\rho_{i,j} + \rho_{i+1,j})$ and $\rho_{i,j+1/2}^{-1} = 2/(\rho_{i,j} + \rho_{i,j+1})$ (Kummer *et al.*, 1987; Moczo *et al.*, 2002; Vishnevsky *et al.*, 2014). Time is discretized by $t^n = t^0 + n\Delta t$ with a constant time step Δt that should obey the Courant–Friedrichs–Lewy (CFL) stability limit $\Delta t \sqrt{(\Delta x)^{-2} + (\Delta z)^{-2}} \max_{i,j} (c_{i,j}) \leq 1$.

The spatial derivatives in equation (2) involve values outside the domain, which should be provided by suitable boundary conditions. In the examples in the next section, a free-surface boundary condition is imposed at $z_{\min} = 0$ by setting $u_{i,0}^n = -u_{i,1}^n$. The other boundaries are assumed to be non-

reflecting. At z_{\max} , the lowest-order boundary condition of Engquist and Majda (1979), their equation (4.2), is imposed:

$$u_{i,j+1}^{n+1} = u_{i,j}^n + \alpha_{i,j} (u_{i,j+1}^n - u_{i,j}^{n+1}), \quad \text{for } j = N_z, \quad (3)$$

where $\alpha_{i,j} = (1 - v_{i,j})/(1 + v_{i,j})$ and $v_{i,j} = c_{i,j} \Delta t / \Delta z$. This represents a second-order implicit time discretization of the equation $\partial u / \partial t = -c \partial u / \partial z$. Note that the lowest-order Higdon condition (Higdon, 1986; Mulder, 1997) provides the same expression. Similar conditions can be imposed at x_{\min} and x_{\max} .

Numerically exact non-reflecting boundary conditions

An alternative to the classic boundary conditions are the numerically exact ones. Here, only the one at one side of a rectangular domain, at $x = x_{\max}$, is considered. For the moment, assume that the other boundaries are, for instance, zero Dirichlet. The original domain can be extended to the right by constant extrapolation of the material properties in the direction perpendicular to the boundary. The enlarged domain consists of the original one, which also will be referred to as

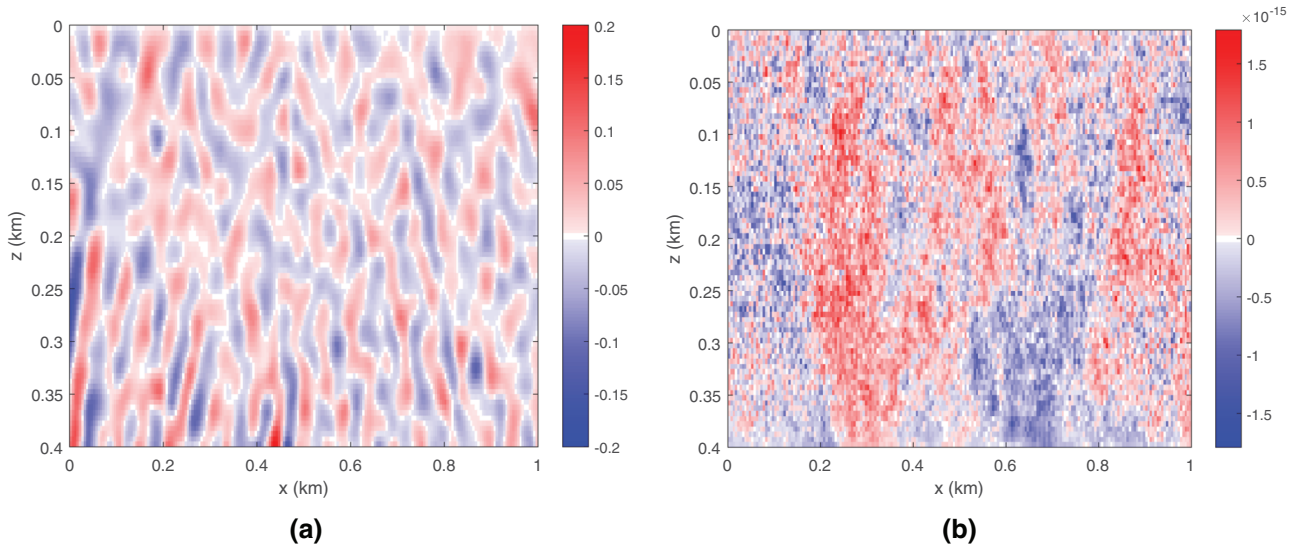


Figure 2 (a) Wavefield after 2 seconds for a random model on the domain extended at x_{\min} and x_{\max} but with Enquist–Majda at the bottom. (b) The difference between the wavefield for numerically exact boundary non-reflecting conditions at x_{\min} and x_{\max} and the Enquist–Majda condition at the bottom and the one in (a) consists in numerical round-off errors.

the interior, and the additional part or exterior. The exterior should be sufficiently large that reflected waves from the new boundary at the right do not have time to reach the original domain.

The non-reflecting boundary condition hinges on the discrete boundary Green functions. These describe, for each point on the boundary, the response in the exterior of unit spikes in time and space on the non-reflecting boundary of the interior. Figure 1 sketches the idea. The domain is split into two parts, the original domain with grid points marked as open circles and the exterior that extends all the way to infinity with grid points drawn as filled black circles. For each interior point on the boundary, with one drawn as a red filled and the other as red open circles, the initial-boundary value problem for the discrete wave equation is solved in the exterior, with at the bottom and top the same boundary conditions as for the interior. At the far right, at infinity, ideally a non-reflecting boundary condition is imposed, but a reflecting will do as well if the simulation time is shorter than the time needed for reflected waves to return to the interior. At the left, the boundary values of the interior are applied, which are set to zero except for the unit spike at time zero at the selected boundary point. Repeating this for each point on the non-reflecting boundary of the interior, marked by the red circles, produces the boundary Green functions.

When convolved in space and time with the actual boundary values present in the interior, the solution in the exterior

is predicted for the next time step and at an arbitrary distance from the boundary. With the lowest-order scheme above, only the points next to the boundary in the exterior are needed, as indicated by the arrows. Then, the discrete wave equation can be evaluated in the interior for the current time step, using the predicted values on the points just outside the boundary as given. In this way, the computation of the response in the exterior part of the domain, excluding the interior except for the single boundary spike at time zero, is decoupled from the simulation in the interior.

A second ingredient of the method is the computation of the discrete boundary Green functions. Simulations in the exterior for each boundary spike will provide them, but at a significant cost. With the assumption of constant extrapolation of the material properties in the direction perpendicular to the boundary, recursion based on translation invariance in combination with the discretized wave equation in a small strip can be applied to compute the boundary Green functions close to the boundary. Their evaluation involves simple expressions but is still costly because of the convolutions in space and time.

Although constant extrapolation perpendicular to the boundary is a reasonable choice, it may cause problems, for instance, in the presence of dipping layers next to the boundary. Horizontal or vertical extrapolation will then create a strong diffractor on the boundary. It is therefore better if the medium is changed to horizontally layered when approaching

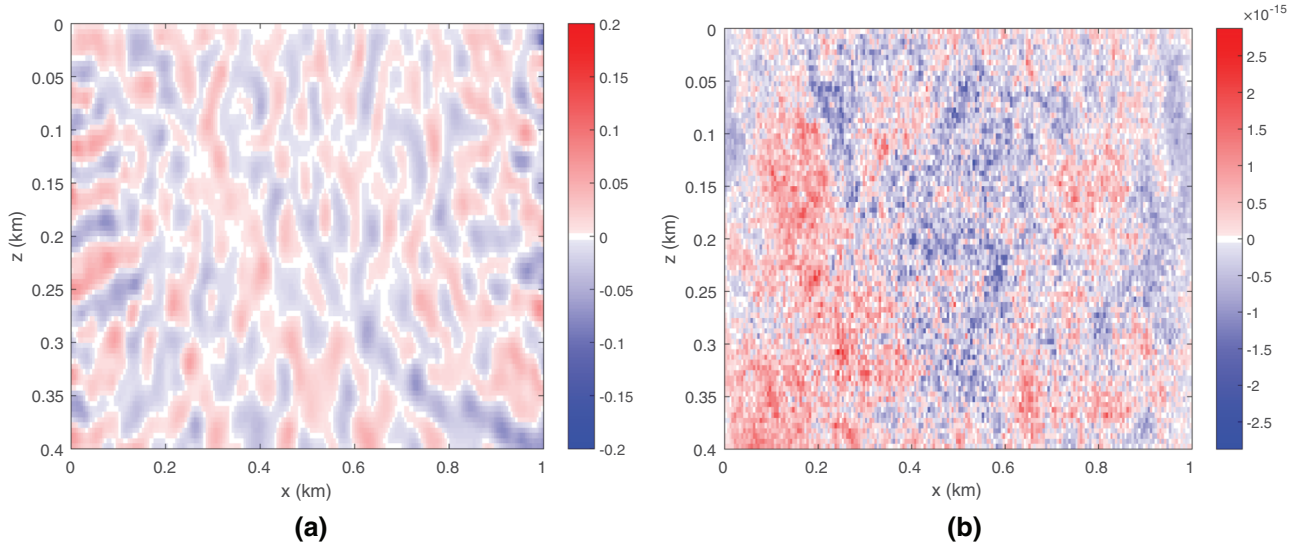


Figure 3 (a) Wavefield for a domain extended at z_{\max} but with Enquist–Majda at the left and right. (b) Difference between the wavefield with the exact condition at z_{\max} and Enquist–Majda at the left and right and the one in (a).

the boundary, or smoothed to avoid large contrasts. Such adaptations represent a research topic by itself and will not be considered further. Instead, we continue with a brief review of the boundary conditions.

The discrete boundary Green function $G_{i,j;N_x,j_0}^n$ for x_{\max} is defined as the wavefield generated by a unit spike at time zero ($n = 0$) and position (x_{N_x}, z_{j_0}) , evaluated at later time t^n , $n > 0$, and at positions (x_i, z_j) , $i > N_x$, for j and $j_0 = 1, \dots, N_z$, while setting the wavefield to zero at $x = x_{N_x}$ for $n > 0$. This means that $G_{N_x,j;N_x,j_0}^n = \delta_{n,0}\delta_{j,j_0}$, using the Kronecker delta. It also implies that these Green functions do not depend on the sound speed and density at $i < N_x$, as long as the time step Δt and grid spacings are kept fixed, as well as the sound speeds and densities at $i = N_x$.

With these Green functions, the wavefield just outside the domain can be predicted from earlier values on the boundary:

$$u_{N_x+1,j}^n = \sum_{m=1}^n \sum_{j_0=1}^{N_z} G_{N_x+1,j;N_x,j_0}^m u_{N_x,j_0}^{n-m}. \quad (4)$$

Note that this expression only holds for the lowest-order discretization. For higher orders, additional points for some values of $i < N_x$ are involved (Mulder, 2020).

The boundary Green functions $G_{i,j;N_x,j_0}^n$ at $i = N_x + 1$ follow from the discrete wave equation (2) with zero source term $f_{i,j}^n = 0$. Constant extrapolation in the direction perpendicular to the boundary is applied to the sound speed and density: $c_{i,j} = c_{N_x,j}$ and $\rho_{i,j} = \rho_{N_x,j}$ for $i > N_x$.

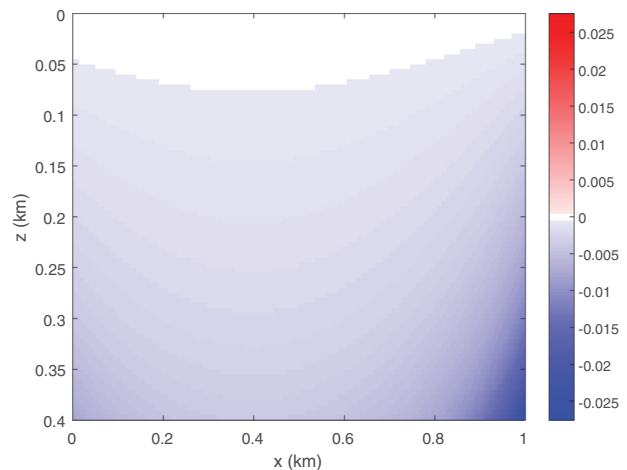


Figure 4 Wavefield for constant model.

Initially, $G_{N_x+1,j;N_x,j_0}^0 = 0$, $G_{N_x+1,j;N_x,j_0}^1 = (c_{N_x,j}\Delta t/\Delta x)^2\delta_{j_0,j}$ and $G_{N_x+2,j;N_x,j_0}^0 = G_{N_x+2,j;N_x,j_0}^1 = 0$.

The discrete wave equation in the strip $i = N_x + 1$ involves values at the left, at $i = N_x$, that are all zero except for the unit spike at time $n = 0$ and position (x_{N_x}, z_{j_0}) . At the top, the free surface can be modelled by anti-symmetric extrapolation: $G_{N_x+1,0;N_x,j_0}^n = -G_{N_x+1,1;N_x,j_0}^n$. At the bottom, the same boundary condition as in the interior should be used, for instance, zero Dirichlet as at the free surface, zero Neumann with $G_{N_x+1,N_z+1;N_x,j_0}^n = G_{N_x+1,N_z;N_x,j_0}^n$ or the Enquist–Majda condition of equation (3), which is the proposed workaround

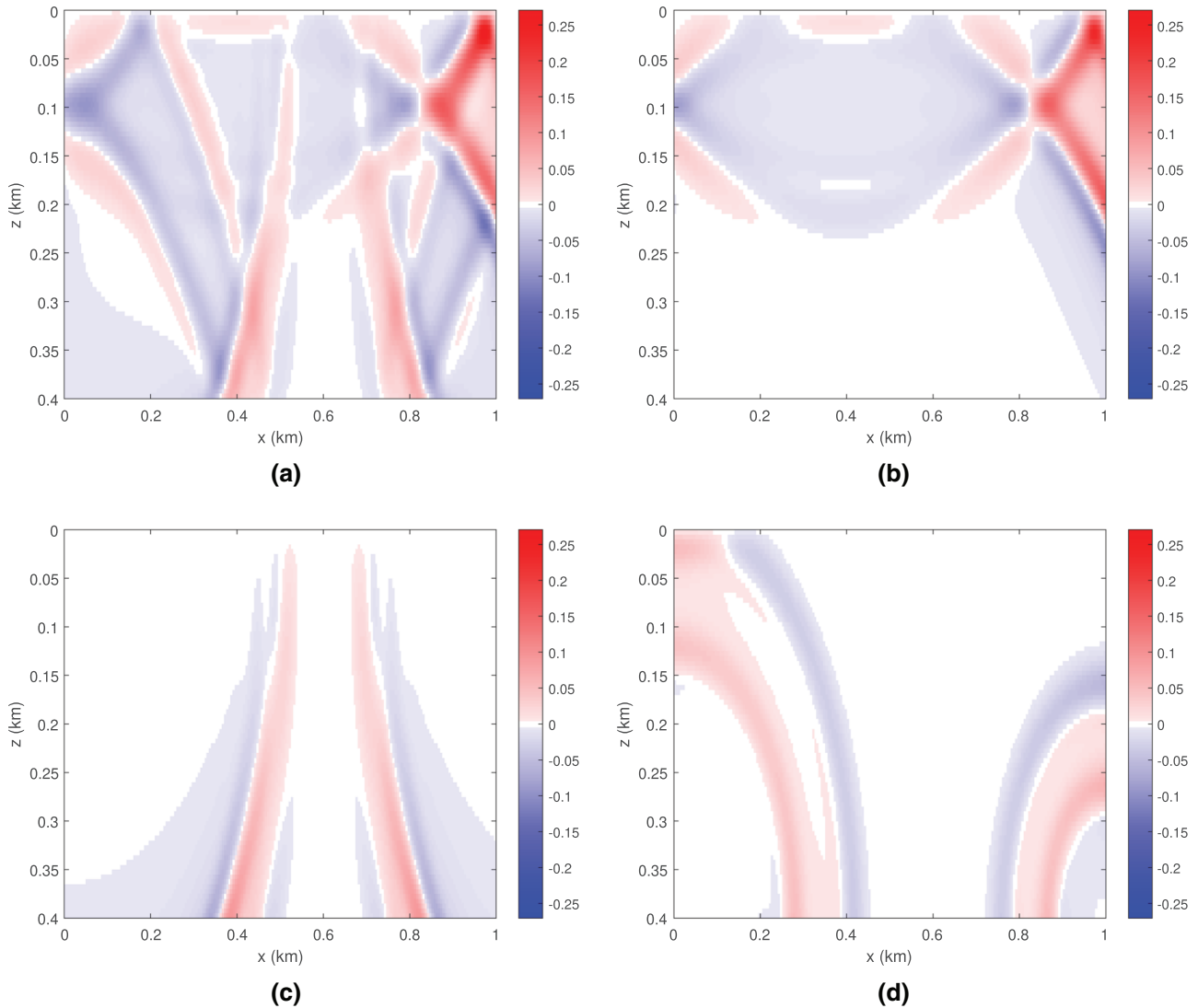


Figure 5 (a) Difference between the wavefield on the truncated and the enlarged domain, as shown in Fig. 4, for (a) Enquist–Majda boundary conditions, (b) exact at x_{\min} and x_{\max} , (c) exact at z_{\max} , and (d) exact, separately at x_{\min} , x_{\max} and z_{\max} . Note that the true solution in Fig. 4 has a smaller amplitude.

in this paper. At the right, at $i = N_x + 2$, recursion with equation (4) shifted one point to the right results in

$$G_{N_x+2, j; N_x, j_0}^n = \sum_{m=1}^{n-1} \sum_{k=1}^{N_z} G_{N_x+1, j; N_x, k}^{n-m} G_{N_x+1, k; N_x, j_0}^m, \quad n > 1. \quad (5)$$

Its earlier values are zero. Note that the last equation assumes translation invariance in the direction perpendicular to the boundary. Alternating between this recursion relation and the discrete partial difference equation at $i = N_x + 1$ provides the boundary Green functions $G_{N_x+2, j; N_x, j_0}^n$ and $G_{N_x+1, j; N_x, j_0}^n$, of which only the latter is needed in equation (4).

Convolution is the most costly part of the method. Sofronov and Podgornova (2006) describe further approximations to reduce that cost, but these have not been considered here. Note that the discrete boundary Green functions can be reused if the material properties on the boundary, the grid spacing and the time step stay the same, which may be useful for simulating multiple shots.

RESULTS

As a proof of principle, a random model on a domain 1 km wide and 40 m deep is considered. Sound speed values vary

between 0.7 and 1.0 km/s, whereas density values range from 0.8 to 2.0 g/cm³. Such a model is pre-eminently suited for code development and testing. The source at $x_s = 397.5$ m and $z_s = 97.5$ m, on a grid point, has a wavelet $w(t) = -\frac{d}{dt}[4(t/T_w)(1 - t/T_w)]^{1/2}$ for $0 \leq t \leq T_w = 0.1625$ s and zero otherwise, which corresponds to a peak frequency of about 10 Hz. The grid spacing is $\Delta x = \Delta z = 5$ m. A free-surface boundary condition is present at $z_{\min} = 0$ m.

A first test had non-reflecting boundary conditions at the left and right, at $x_{\min} = 0$ and $x_{\max} = 1$ km, and the Enquist–Majda conditions at the bottom. For comparison, a run was performed on a domain extended at the left and right but with a free surface at the top and the Enquist–Majda conditions at the bottom. Figure 2(a) shows a subset of the resulting wavefield after 2 seconds. The difference between the result with the numerically exact non-reflecting boundary conditions at the left and right and a subset of the former is shown in Fig. 2(b) and is of the order of 10^{-15} , representing accumulated numerical round-off errors in a double-precision computation.

Figure 3(a) shows the wavefield for a second test, now with the Enquist–Majda boundary conditions at the left and right and a non-reflecting boundary at the bottom, at $z_{\max} = 0.4$ km. Again, the difference with the wavefield for a numerically exact non-reflecting boundary condition at the bottom consists in numerical round-off noise, as shown in Fig. 3(b). This demonstrates the effectiveness of the exact boundary conditions and the correctness of the code.

The second example is a constant model with a sound speed of 1 km/s and density of 1 g/cm³. Again, the boundaries are non-reflecting except for the free surface at $z_{\min} = 0$ m. Domain size, shot position and wavelet are the same as in the first example. Figure 4 shows a subset of the wavefield on the original domain after 1 second, computed on an domain enlarged in both x and z . The wavefront has already disappeared and only the tail of the two-dimensional Green function is visible.

Figure 5 shows the difference between the wavefield for various boundary conditions with that of Fig. 4. Figure 5(a) displays the result for Enquist–Majda boundary conditions on all sides except the free surface. With numerically exact conditions at the left and right but Enquist–Majda at the bottom, the result of Fig. 5(b) is obtained. The approximate character of the Enquist–Majda condition generates reflected waves at the bottom that travel back to the surface, where they are reflected by the free surface. The figure shows the remnants of these up- and downgoing waves. With an exact condition at the bottom, at $z_{\max} = 400$ m and Enquist–Majda on the left and right, Fig. 5(c) is obtained. Now, we see horizontally

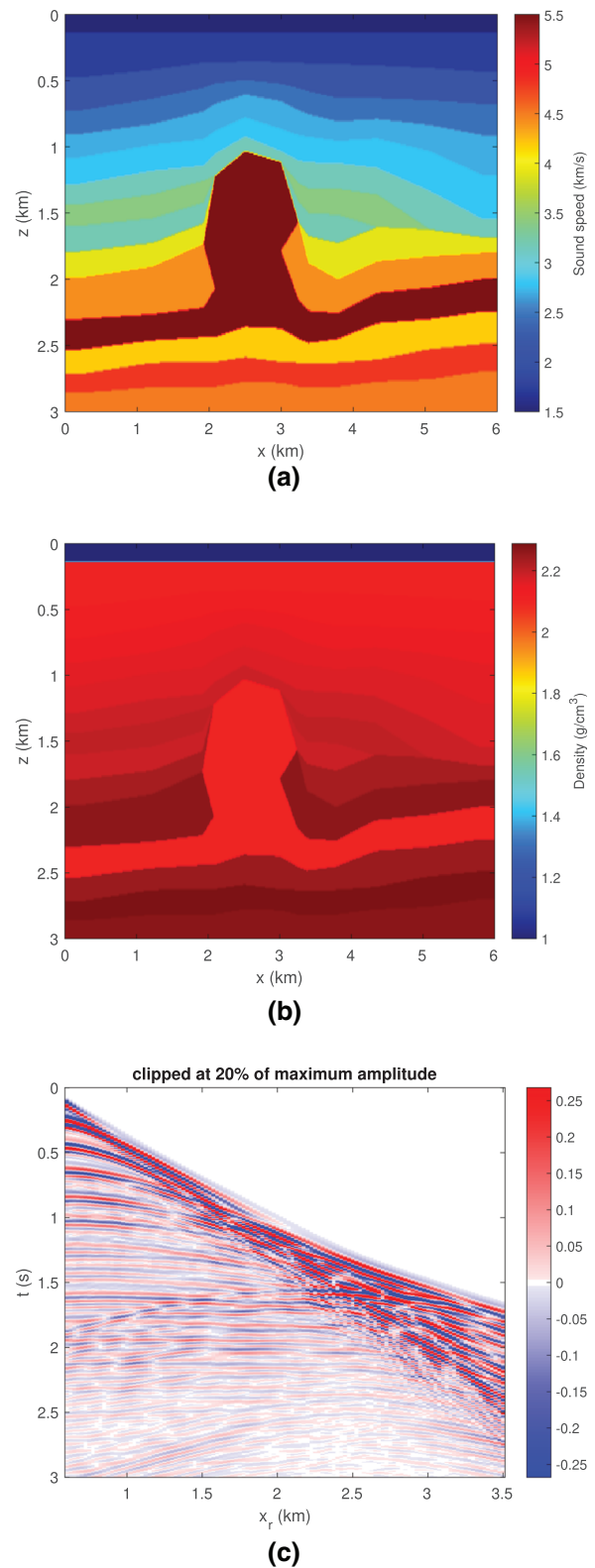


Figure 6 (a) Sound speed model. (b) Density. (c) Seismogram.

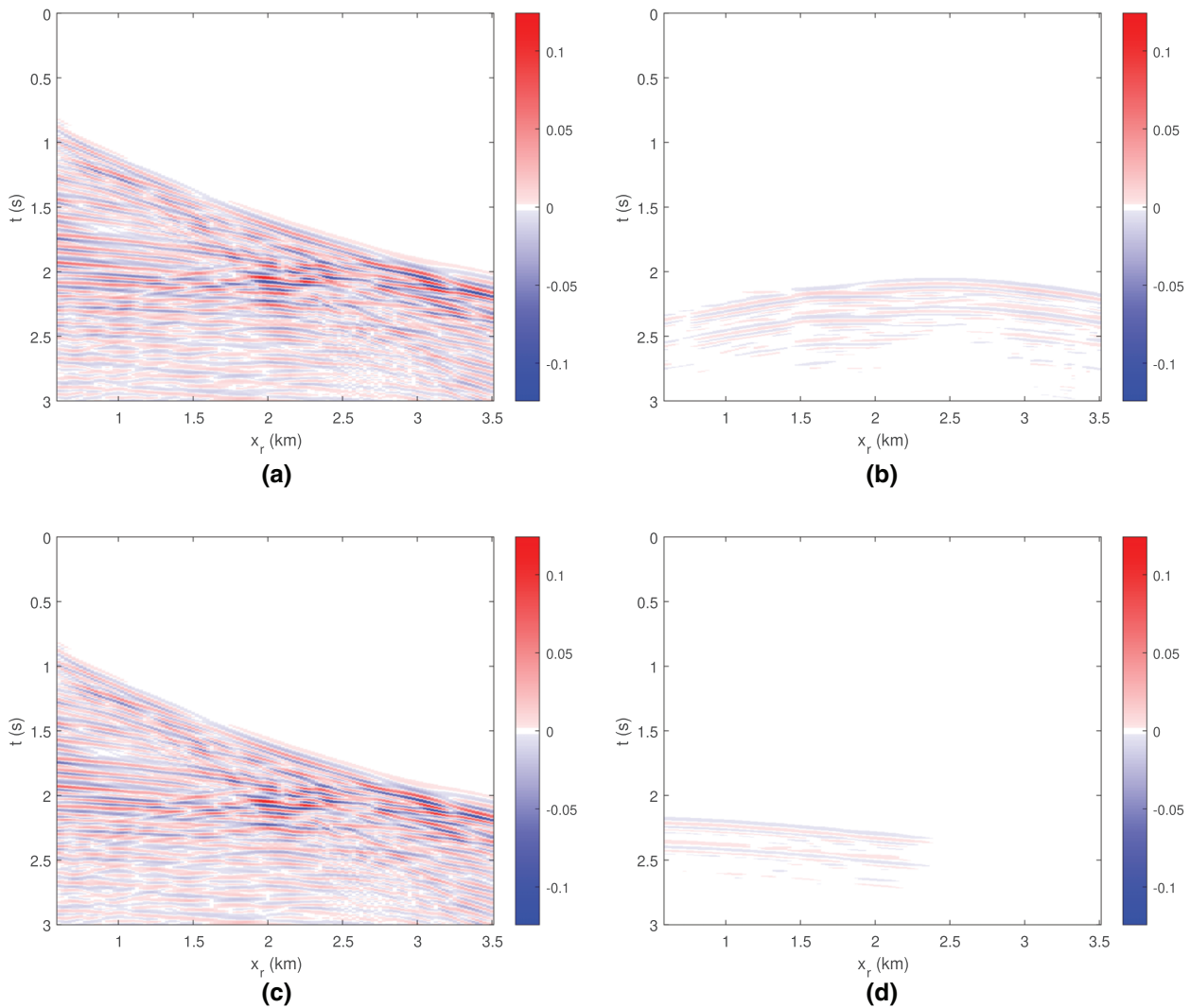


Figure 7 Difference between the seismogram on the truncated and the enlarged domain, shown in Fig. 6(c), for (a) Enquist–Majda boundary conditions, (b) exact at x_{\min} and x_{\max} , (c) exact at z_{\max} and (d) exact, separately at x_{\min} , x_{\max} and z_{\max} .

travelling waves caused by the inexactness of the boundaries on the left and right.

If the exact boundary conditions are applied independently, assuming an Enquist–Majda or free-surface boundary condition in the other direction during the computation of the discrete boundary Green functions, the result of Fig. 5(d) is obtained. The difference with the one in Fig. 4 now mainly consists in waves reflected from the corner. Note that all the figures have the same scale. The actual maximum amplitudes for the various runs are: 0.028 for the full wavefield on the extended domain, 0.27 for the *difference* plot in Fig. 5(a) with the Enquist–Majda conditions, 0.24 for the difference plot with exact conditions in x (b), and 0.095 with exact conditions in z (c), showing that the waves reflected from the bottom are

strongest in this example. The maximum amplitude of the difference when exact conditions are applied independently in x and z is 0.064, mainly caused by waves reflected from the two corners at the bottom, visible in Fig. 5(d). The corner reflection is caused by the approximate character of the Enquist–Majda conditions employed in the discrete wave equation during the computation of the boundary Green functions.

The third and last example is a salt diapir in a marine environment with a shallow sea, slightly modified from Mulder (2001). Figure 6(a,b) shows the velocity model and the density. Figure 6(c) displays the seismogram for a shot at $x_s = 505$ m and $z_s = 15$ m for the same wavelet as in the previous example but now with $T_w = 1.625/f_{\text{peak}}$, $f_{\text{peak}} = 12$ Hz. Receivers were placed at a depth of 10 m between $x_r = 600$

and 3500 m at a 25-m interval. The grid spacing was 10 m. Figure 7(a) plots the difference between a seismogram determined with the Enquist–Majda boundary conditions on all sides except the free surface and the seismic data obtained on the enlarged domain of Fig. 6(c). Figure 7(b) shows the difference with exact conditions at the left and right and Enquist–Majda at the bottom. Only reflected waves from the bottom, caused by the approximate character of the Enquist–Majda boundary conditions, are visible. With an exact boundary at the bottom and Enquist–Majda on the left and right, the result in Fig. 7(c) resembles that of Fig. 7(a), indicating that with Enquist–Majda, the stronger reflected events come from the side. Finally, Fig. 7(d) displays the result with exact boundary conditions applied independently. Note that all graphs of Fig. 7 employ the same scale. The maximum observed amplitudes, scaled by that of the result in Fig. 6(c), are 0.093 for Enquist–Majda, 0.010 with exact boundaries in x , 0.092 with an exact boundary at z_{\max} and 0.0050 with independent exact boundaries at x_{\min} , x_{\max} and z_{\max} . From a cost perspective, exact conditions only in x may be preferable in this example.

CONCLUSIONS


Numerically exact non-reflecting boundaries provide a solution that is not different from one on an enlarged domain with the boundary so far away that unwanted reflected waves do not have time to return. They require discrete boundary Green functions that can be computed by a simple recurrence relation if only one or two opposing sides of a rectangular domain are considered, assuming that material properties in the enlarged domain are obtained by constant extrapolation in the direction perpendicular to the boundary. If two sides share a common corner, translation invariance is lost and a simple recurrence relation does not seem to exist. The proposed workaround consists of an exact condition in one direction and a classic, approximate condition in the other. Although exactness is lost, the resulting condition can be advantageous in cases where the classic conditions provide reflection events that are much stronger in one coordinate direction than in the other. This can happen in the presence of a shallow water layer or with strong surface waves. Alternatively, the exact conditions can be applied independently, using the approximate conditions in the other direction during the recursive computation of the boundary Green functions. This leaves reflected waves from the corners. In the examples studied, these have significantly smaller amplitudes than the reflected waves from the sides generated by the approximate classic boundary condition used, the lowest-order Enquist–Majda condition.

Higher-order finite-difference discretizations are feasible, as well as a combination with higher-order approximately non-reflecting boundary conditions. A disadvantage of the proposed boundary condition is the computational cost, caused by its convolutional character. However, the boundary Green functions can be reused for a several problems as long as the grid size, time step and material properties next to or on the boundaries do not change.

DATA AVAILABILITY STATEMENT

Data sharing is not applicable to this article as no new data were created or analysed in this study. However, if the computational results shown in the figures are considered as new data, then the author elects not to share those.

ORCID

W.A. Mulder  <https://orcid.org/0000-0001-7020-9297>

REFERENCES

- Antoine, X., Lorin, E. and Tang, Q. (2017) A friendly review of absorbing boundary conditions and perfectly matched layers for classical and relativistic quantum waves equations. *Molecular Physics*, 115(15–16), 1861–1879. <https://doi.org/10.1080/00268976.2017.1290834>
- Bérenger, J.-P. (2015) A historical review of the absorbing boundary conditions for electromagnetics. *Forum for Electromagnetic Research and Application Technologies (FERMAT)*, 9, 1–28. <https://www.e-fermat.org/files/articles/154db8c5adee49.pdf>
- Deakin, A. and Dryden, J. (1995) Numerically derived boundary conditions on artificial boundaries. *Journal of Computational and Applied Mathematics*, 58(1), 1–16. [https://doi.org/10.1016/0377-0427\(93\)E0261-J](https://doi.org/10.1016/0377-0427(93)E0261-J)
- Engquist, B. and Majda, A. (1979) Radiation boundary conditions for acoustic and elastic wave calculations. *Communications on Pure and Applied Mathematics*, 32(3), 313–357. <https://doi.org/10.1002/cpa.3160320303>
- Gao, Y., Song, H., Zhang, J. and Yao, Z. (2017) Comparison of artificial absorbing boundaries for acoustic wave equation modelling. *Exploration Geophysics*, 48(1), 76–93. <https://doi.org/10.1071/EG15068>
- Givoli, D. (2004) High-order local non-reflecting boundary conditions: a review. *Wave Motion*, 39(4), 319–326. <https://doi.org/10.1016/j.wavemoti.2003.12.004>
- Givoli, D. and Cohen, D. (1995) Nonreflecting boundary conditions based on Kirchhoff-type formulae. *Journal of Computational Physics*, 117(1), 102–113. <https://doi.org/10.1006/jcph.1995.1048>
- Givoli, D., Patlashenko, I. and Keller, J. B. (1998) Discrete Dirichlet-to-Neumann maps for unbounded domains. *Computer Methods in Applied Mechanics and Engineering*, 164(1), 173–185. [https://doi.org/10.1016/S0045-7825\(98\)00053-X](https://doi.org/10.1016/S0045-7825(98)00053-X)

- Hagstrom, T. and Lau, S. (2007) Radiation boundary conditions for Maxwell's equations: a review of accurate time-domain formulations. *Journal of Computational Mathematics*, 25(3), 305–336. <https://www.jstor.org/stable/43693369>
- Higdon, R. L. (1986) Absorbing boundary conditions for difference approximations to the multi-dimensional wave equation. *Mathematics of Computation*, 47(176), 437–459. <https://doi.org/10.2307/2008166>
- Keller, J. B. and Givoli, D. (1989) Exact non-reflecting boundary conditions. *Journal of Computational Physics*, 82(1), 172–192. [https://doi.org/10.1016/0021-9991\(89\)90041-7](https://doi.org/10.1016/0021-9991(89)90041-7)
- Kummer, B., Behle, A. and Dorau, F. (1987) Hybrid modeling of elastic-wave propagation in two-dimensional laterally inhomogeneous media. *Geophysics*, 52(6), 765–771. <https://doi.org/10.1190/1.1442343>
- Mitra, R., Ramahi, O. O., Khebir, A., Gordon, R. and Kouki, A. (1989) A review of absorbing boundary conditions for two and three-dimensional electromagnetic scattering problems. *IEEE Transactions on Magnetics*, 25(4), 3034–3039. <https://doi.org/10.1109/20.34361>
- Moczo, P., Kristek, J., Vavryčuk, V., Archuleta, R. J. and Halada, L. (2002) 3D heterogeneous staggered-grid finite-difference modeling of seismic motion with volume harmonic and arithmetic averaging of elastic moduli and densities. *Bulletin of the Seismological Society of America*, 92(8), 3042–3066. <https://doi.org/10.1785/0120010167>
- Mulder, W. A. (1997) Experiments with Higdon's absorbing boundary conditions for a number of wave equations. *Computational Geosciences*, 1(1), 85–108. <https://doi.org/10.1023/A:1011556926362>
- Mulder, W. A. (2001) Higher-order mass-lumped finite elements for the wave equation. *Journal of Computational Acoustics*, 9(2), 671–680. <https://doi.org/10.1142/S0218396X0100067X>
- Mulder, W. A. (2020) Exact non-reflecting boundary conditions with an FDTD scheme for the scalar wave equation in waveguide problems. *Progress in Electromagnetics Research M*, 91, 39–48. <https://doi.org/10.2528/PIERM19121202>
- Sofronov, I. L. and Podgornova, O. V. (2006) A spectral approach for generating non-local boundary conditions for external wave problems in anisotropic media. *Journal of Scientific Computing*, 27, 419–430. <https://doi.org/10.1007/s10915-005-9041-0>
- Teng, Z.-H. (2003) Exact boundary condition for time-dependent wave equation based on boundary integral. *Journal of Computational Physics*, 190(2), 398–418. [https://doi.org/10.1016/S0021-9991\(03\)00281-X](https://doi.org/10.1016/S0021-9991(03)00281-X)
- Ting, L. and Miksis, M. J. (1986) Exact boundary conditions for scattering problems. *The Journal of the Acoustical Society of America*, 80(6), 1825–1827. <https://doi.org/10.1121/1.394297>
- Tourrette, L. and Halpern, L. (2001) *Absorbing Boundaries and Layers, Domain Decomposition Methods: Applications to Large Scale Computers*. Hauppauge, NY: Nova Science Publishers, Inc.
- Tsynkov, S. V. (1998) Numerical solution of problems on unbounded domains. A review. *Applied Numerical Mathematics*, 27(4), 465–532. (Special issue on absorbing boundary conditions.) [https://doi.org/10.1016/S0168-9274\(98\)00025-7](https://doi.org/10.1016/S0168-9274(98)00025-7)
- van Manen, D., Robertsson, J. O. A. and Curtis, A. (2007) Exact wave field simulation for finite-volume scattering problems. *The Journal of the Acoustical Society of America*, 122(4), EL115–EL121. <https://doi.org/10.1121/1.2771371>
- Vishnevsky, D., Lisitsa, V., Tcheverda, V. and Reshetova, G. (2014) Numerical study of the interface errors of finite-difference simulations of seismic waves. *Geophysics*, 79(4), T219–T232. <https://doi.org/10.1190/geo2013-0299.1>